9

Design Efficiency of ESP

Maria Jędrusik and Arkadiusz Świerczok
Wroclaw University of Technology
Poland

1. Introduction

Electrostatic precipitator (ESP) is a highly efficient device for cleaning exhaust gases from industrial processes. Fig. 1 shows a photograph of electrostatic precipitator (ESP) for cleaning flue gases from a power boiler, and Fig. 2 shows the inner part of the ESP.

The basic components of ESP are: a chamber comprising discharge and collection electrodes, and high voltage (HV) supply unit - shown in Fig. 3. The ESP operation is based on the utilization of the influence of electric field on charged dust particles flowing between the electrodes. The Discharge electrodes (DE) are connected to a direct current (DC) HV power supply of negative polarity and the collecting electrodes to the positive pole of the supply, which is additionally grounded. The raw exhaust gas is subjected to electron and ion currents which charge the dust particles negatively, and cause their movement towards the collecting electrode. The precipitation of dust particles from a gas stream as well as its collection occurs mainly because of the electrophoresis forces.

Fig. 1. Electrostatic precipitator in Thermal-Power Station.

Fig. 2. Inner part of the ESP.

Dust particles collected on the CE surfaces partly give up their charge and the dust layer is kept on the CE electrodes by means of mechanical and electrical forces. Afterwards the collected dust layer is knocked down mostly by mechanical rapping systems.

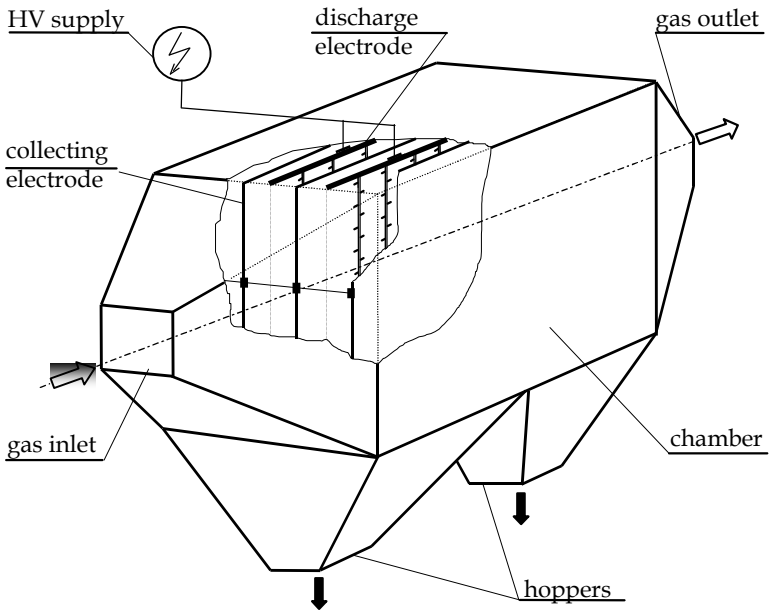

Fig. 3. Typical arrangement of wire-and-plate precipitator with horizontal gas flow.

2. Kinetics of dust particle charging

The dust particles in ESP are charged as a result of taking over the electric charge from gaseous ions. The source of gas ionization is a negative corona discharge originating at the DEs.

The discharge takes place due to strongly inhomogeneous electric field in the vicinity of appropriately formed DE surface, for example, in the form of thin round wire or a similar element with mounted spikes. The empirical equation of the corona-onset electric field strength on DE spikes has been given by Peek (Peek, 1929).

$$E_o = A\delta + B\sqrt{\frac{\delta}{r_o}} \tag{1}$$

where:

- E_o – initial electric field strength, V/m
- A, B – experimental coefficients characterizing gas type and discharge polarity. For an ESP with negative discharge polarity Robinson (Parker, 1997) advices to use empirical values: A=3.2·10^6 V/m, B=9·10^4 V/m^{½},
- r_o – DE curvature radius, m
- δ – relative density of gas, -

The magnitude of supply voltage at which the corona discharge begins on the DE surface is called the corona onset voltage. Above this level, develop the electron avalanches from the discharge electrode towards the plate. The electrons emitted from the spikes are accelerated in the strong electric field and gain energy necessary for avalanche ionization of atoms and gaseous molecules. Additional source of electrons in the discharge is also the so called secondary emission due to positive ions impacting the DE. The avalanches originating from DE develop in the direction of CE. Electrons from the avalanche head are quickly attach to neutral gas molecules , which-become negative gas ions. Dust particles get electric charge due to non-elastic collisions with negative as well as positive gas ions. In the charging process of dust particles, two distinguish basic mechanisms are considered (White, 1990):

- field charging,
- diffusion charging.

An equation describing the charge on a dielectric spherical particle for the field charging mechanism has been given by Pauthenier and Moreau-Hanot (Pauthenier & Moreau-Hanot, 1932) in the following form:

$$q_f = q_s \cdot \frac{t}{t+\tau} \tag{2}$$

where: q_f – particle charge obtained from field charging,

$$q_s = \pi\varepsilon_o \frac{3\varepsilon_w}{\varepsilon_w + 2} E d^2 \quad \text{– particle saturation charge,}$$

$$\tau_f = \frac{4\varepsilon_o E}{j} \quad \text{– field charging constant,}$$

- ε_w – dielectric constant of particle material ,
- ε_o – dielectric constant of free space $\left(8.85 \cdot 10^{-12} \frac{C^2}{Nm^2}\right)$
- E – electric field strength,
- t – charging time,
- d – particle diameter.

White in 1963 (White, 1990) has given the equation of particle charging for diffusion mechanism in the form of:

$$q_d = \frac{2\pi \varepsilon_o kTd}{e} \ln\left(1 + \frac{t}{\tau_d}\right) \tag{3}$$

where:

- q_d – particle charge obtained from diffusion charging
- k –Boltzmann constant ($1.38 \cdot 10^{-23}$ J/K)
- T – temperature
- e – electron charge, ($e = 1.67 \cdot 10^{-19}$ C)
- τ_d – diffusion charging constant

$$\tau_d = \frac{\varepsilon_o \sqrt{8 m_j k \pi T}}{e^2 N d} \tag{4}$$

- N – number of unipolar ions in the unit volume (ion density)
- m –mass of an ion

It was experimentally demonstrated that a total charge of dust particle can calculated with practically sufficient accuracy as a sum of field charge (2) and diffusion charge (3).

$$q_p(t) = q_f(t) + q_d(t) \tag{5}$$

It should be noted that all of the above mentioned charging theories apply only to spherical particles. When taking into account industrial dust particles it is necessary to use their equivalent dimensions (diameter).

In typical industrial ESP, the dust size distribution at the precipitator inlet does not comprise fine particles –below 4 μm, and the electric field is usually over 1 kV/m. Therefore, based on the research results presented in the literature, it is generally accepted that the mechanism of diffusion charging may be ignored. This also proves that the Pauthenier's & Moreau-Hanot equation describes the kinetics of dust particle charging with sufficient accuracy.

3. Dust particle motion in ESP

In order to characterize the movement of charged particle in an ESP it is necessary to assume the equilibrium of forces acting on the particle. After some simplifications it can be said that the following forces are acting on a dust particle in an ESP: the inertia force, electric force and drag force of the medium, where:

$$\vec{F}_i = -m \cdot \frac{d\vec{u}}{dt} \tag{6}$$

$$\vec{F}_e = q_s \cdot \vec{E} \tag{7}$$

$$\vec{F}_d = c_d(\mathrm{Re}) \cdot \rho_g \cdot \frac{\pi d}{8}(\vec{v} - \vec{u})|\vec{v} - \vec{u}| \tag{8}$$

The motion of any dust particle may be described as by the Newton second law:

$$\vec{F}_i + \vec{F}_e + \vec{F}_d = 0 \tag{9}$$

The scheme of particle motion in electric field illustrates Fig. 4.

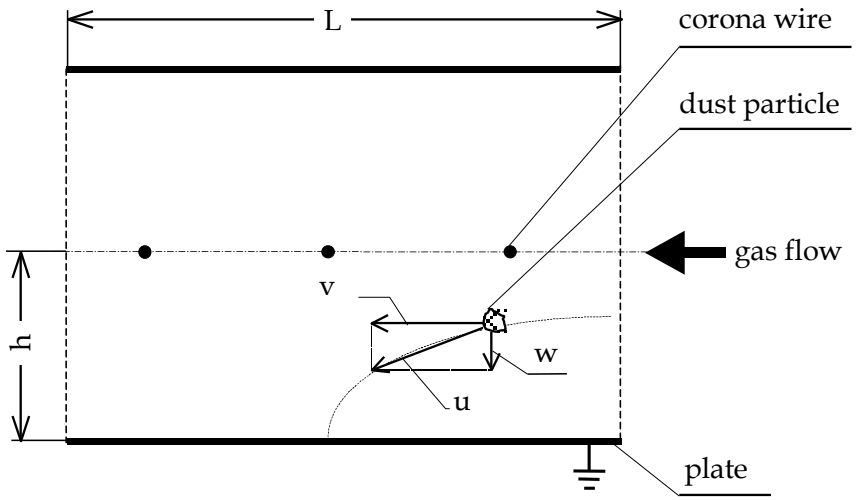

Fig. 4. Schematic diagram of particle motion in electric field (plate to plate configuration).

In the vector form, the equation of motion becomes:

$$m\frac{d\vec{u}}{dt} = -c_d(\mathrm{Re})\,\rho_g \frac{\pi d}{8}(\vec{v} - \vec{u})|\vec{v} - \vec{u}| + q_s\vec{E} \tag{10}$$

where:

- $\vec{v}$ - vector of gas velocity
- $\vec{u}$ - vector of particle velocity
- ρ_g - gas density
- $\vec{v}-\vec{u}$ - particle velocity in relation to gas velocity
- $c_d(Re)$ – dynamic drag coefficient
- m – particle mass

It should be emphasized that the dominant role in this equation play the electric force and drag force of the gas medium. In the steady state motion the inertia force can be omitted because of its low value comparing to the electric force (Parker, 1997).

The equation (10) finally gets the form:

$$-c_d(\mathrm{Re})\cdot\rho_g\frac{\pi d}{8}(\vec{v}-\vec{u})\left|\vec{v}-\vec{u}\right|+q_s\vec{E}=0 \tag{11}$$

3.1 Theoretical migration velocity

Accepting for further consideration the simplest case of spherical particle steady motion in electric field –in the range of Stoke's law (Re ≤ 0.1), equation (11) can be transformed to the form:

$$q_sE-3\pi\mu d\cdot w=\mathbf{0} \tag{12}$$

where: w – particle relative velocity normal to CE surface; so called migration velocity $w=(\vec{v}-\vec{u})$

Theoretical value of the migration velocity, calculated from equation (12) equals to:

$$w=\frac{q_s\cdot E}{3\pi\mu d} \tag{13}$$

The minimum range of the size of particles to which the Stoke's equation can be applied is the case when the particle diameter is of the order of magnitude of mean free path of gas molecules $\bar{\lambda}$. For particles smaller than 1 μm it is necessary to take into account the Cunningham slip correction factor:

$$w=\frac{q_sEC_u}{3\pi\mu d} \tag{14}$$

where:

C_u - Cunningham slip correction factor (White, 1990); $\quad C_u=1+0.86\frac{2\bar{\lambda}}{d}$

The formulas used for the calculation of theoretical migration velocity do not take into account many factors affecting the movement of dust particle in electric field such as:

inertia, inhomogeneity of electric field strength distribution, gas velocity, and electric wind velocity.

In the electrostatic precipitation process with a spike and plate electrodes arrangement there exists an electro-hydro-dynamic (EHD) flow, which is an effect of mutual interaction of electrically neutral main gas stream and gas ions movement under the influence of electric field. To describe such flow field it is necessary to use dimensionless parameters determined by IEEE-DEIS-EHD Technical Commitee (IEEE-DEIS-EHD TC, 2003).

$$\mathrm{Re} = \frac{L \cdot \overline{v}}{\nu} \tag{15}$$

$$Ehd = \frac{L^3 \cdot j_0}{\nu \cdot \rho_g \cdot b \cdot A} \tag{16}$$

$$Md = \frac{\varepsilon_0 \cdot E_0{}^2 \cdot L^2}{\rho_g \cdot \nu} \tag{17}$$

where:

- L – characteristic length, i.e. distance between the electrodes, m
- j_0 –total discharge current, A
- $\overline{v}$ - average gas velocity, m/s
- ν – kinematic viscosity coefficient, m^2/s
- Md – the Masuda number,
- Re – the Reynolds number,
- b – ions mobility: $1.8 \cdot 10^{-4}$, m^2/Vs
- Ehd – electro-hydro-dynamic (EHD) number,
- E_0 – field strength at corona onset, V/m
- ρ_g – gas viscosity, kg/m^3
- A – CE surface for discharge current calculations, m^2

For specified ESP arrangement, the Reynolds number depends on gas flow velocity, and the EHD and Masuda numbers are the functions of discharge voltage, field geometry, and ionization parameters of the gas.

3.2 ESP precipitation efficiency

The basic equation describing precipitation efficiency from the probability theory has been given in 50-ties by White (White, 1990) and latter modified by Matts & Oehnfeld to the following form:

$$\eta(d) = 1 - \exp\left\{-w_t(d) \cdot \frac{L}{h \cdot v}\right\} \tag{18}$$

where:

- $\eta(d)$ – precipitation efficiency for a particle with diameter d,

- $w_t(d)$ –theoretical migration velocity, m/s
- L - length of electric field, m
- h – wire-plate distance, m

The total precipitation efficiency $\eta_C(d)$ can be calculated from the formula:

$$\eta_C(d) = \sum_{d_{\min}}^{d_{\max}} q_3(d)\eta(d) \tag{19}$$

Often an alternative way to determine the total efficiency of precipitation is calculate it by measuring the dust concentration before and after ESP.

4. The influence of combustion process and fired coal parameters on physical & chemical properties of generated fly ash

4.1 Chemical composition of fly ash

The fly ash collected in an ESP is a mixture of different compounds, mainly of silicon and aluminum oxides with average substitute diameter of about 15 μm and submicron particles with diameter below 1 μm (ca. 2wt.%). Characteristic properties of fly ash having the greatest influence on ESP operation are (Parker, 1997): diameter, form and structure of particles, their propensity for agglomeration and cohesion, electrical resistivity, chemical composition and reactivity. The chemical composition of fly ash allows to estimate its predictable electrical resistivity value and, by this way, the required size of the ESP (Chambers et al., 2001). Actually, it often becomes necessary to adapt an existing ESP to new (changed) operational conditions, for example, after installing flue gas desulfurization equipment (Parker, 1997). Also the installation of low-emission burners in boiler results in increasing amount of combustible elements in fly ash (LOI). In that case takes place, changes of the gas-dust medium parameters as well as its electric resistivity can be expected. Former experiences with the electrostatic gas cleaning process led to the conclusion that the dust electrical resistivity is an important parameter influencing the operational efficiency of ESPs. If the dust electric resistivity exceeds 10^{11}–10^{13} Ω·cm it is the so called high resistivity dust, which is difficult to collect. If the resistivity lies between 10^{10}–10^{11} Ω·cm, it is in the optimal range for the collection. The chemical composition of fly ash is closely related to the coal quality. An increase of silicon and alumina compounds in the fly ash (SiO_2, Al_2O_3) may lead to the increase of fly ash electric resistivity and by that to decrease of the ESP collection efficiency. It has been observed that for brown coal fly ash, the electric resistivity increases as the percentage of alkali compounds (CaO + MgO) exceeds 3-6 times that of iron trioxide (Fe_2O_3). However, significant amount of sodium and potassium compounds in fly ash cause a decrease in its resistivity that is particularly noticeable by high content of (SiO_2 + Al_2O_3) (Bibbo, 1994; Bickelhaupt, 1985; Parker, 1997).

A substantial influence on the fly ash electric resistivity has the content of sulphur trioxide in the flue gas entering into ESP, as shown on Fig 5. When firing coal in a combustion chamber, the sulphur contained in the coal is oxidized to SO_2. Depending on the combustion conditions, 0.5-3% of that sulphur dioxide is further oxidized to SO_3. At the temperature of

sulphur acid dew point, the condensation of SO_3 on particle surfaces takes place – or more precisely- H_2SO_4 is formed on it in the form of very thin film.

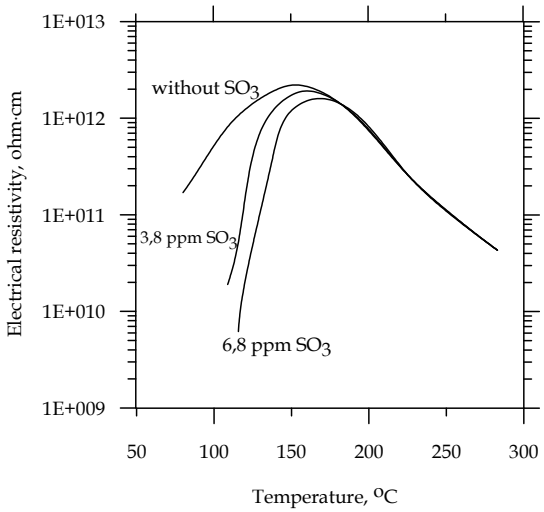

Fig. 5. Electric resistivity of fly ash as a function of SO_3 injection (Parker, 1997).

In Table 1 are presented selected characteristic parameters of fly ash resulting from combustion of hard coal and brown coal in different power boilers.

Chemical composition, %	Fly ash type							
	E	D	B	C	W	A	JG	G
SiO_2	*54.0*	41.00	41.60	37.60	45.67	54.20	47.44	28.99
Fe_2O_3	4.21	10.30	6.50	7.01	8.94	5.30	6.91	3.67
Al_2O_3	4.42	30.60	21.90	21.60	21.65	32.10	19.65	17.14
TiO_2	1.03	2.08	0.85	0.81	1.09	1.40	0.99	0.86
CaO	25.90	3.03	11.90	14.30	8.23	0.81	3.98	2.82
MgO	4.43	1.97	2.29	2.47	2.60	1.09	1.41	1.01
SO_3	4.72	2.80	6.27	6.58	1.57	0.27	0.73	2.26
K_2O	0.24	1.28	2.24	1.87	4.83	2.65	3.03	2.68
P_2O_5	0.26	0.22	0.15	0.16	-	0.55	0.01	0.01
Na_2O	0.09	3.61	1.22	1.48	1.32	0.48	1.33	1.14
Un-burned coal	0.63	0.14	2.38	2.68	3.50	0.61	13.77	28.60
Density, kg/m^3	2500	1954	2580	2690	2210	2031	1550	1580
Resistivity, Ω·cm	4.4×10^8	3.2×10^7	2.0×10^8	1.8×10^8	3.2×10^7	1.8×10^8	5.1×10^7	5.0×10^7

Table 1. Properties of fly ashes.

The influence on chemical composition of fly ash have the quality of fired coal and the combustion parameters. Because both of the mentioned parameters vary with time, the chemical composition of fly ash is also changed with time.

4.2 Dust particle size distribution

Knowledge of the particle size (granulation) distribution is essential to estimate an ESP collection efficiency. The fly ashes coming after combustion of solid fuels are polydisperse and diameter of the particles ranges from fractions of micrometer up to several millimeters. Determination of particles size is a difficult task because of various shapes of the particles, from spherical forms -created as an effect of sublimation and condensation, spatially expanded, inside-empty structures of un-burned coal, snow-flake like flat particles, to fibrous particles. In order to compare the dust size distributions, a equivalent particle diameter has been introduced. It depends on the method of size analysis: the projected diameter (determined by the analysis under projecting microscope or by sieve analysis) or dynamic diameter (obtained using the blow away method in counter-flow, or sedimentation).

The fly ash size distribution is most often presented as fraction of particles $q_r(d_i)$ in a range from d_i to $d_i + \mathrm{d}d$, or the total number of particles $Q_r(d_i)$ smaller than d_i (cumulative size distribution). The particle distribution in a certain size range may be represented by its mass, volume or number ratios. These ratios are called the mass, volumetric and number fractions with the index r equal to 3 (mass and vol.) or 0 (number), respectively (Masuda et al., 2006).

Examples of fly ash size distribution coming from different boilers fired with hard or brown coal are presented in Figs. no 6, 7 & 8. The analysis has been done with an automatic particle size analyzer *Mastersizer S* made by *Malvern Instruments Ltd*. Results of the presented analyses show that the combustor type (boiler type) is a crucial element in forming the fly ash size distribution character.

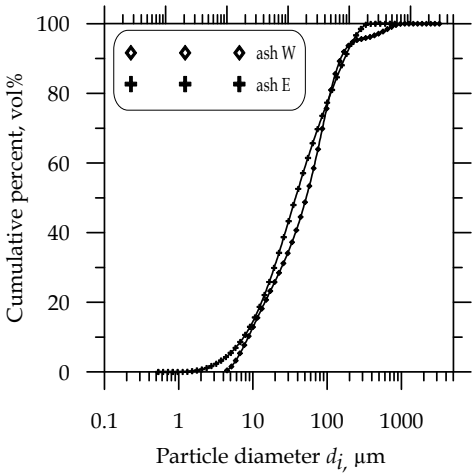

Fig. 6. Particle size distribution $Q_3(d_i)$ of fly ashes from PC boilers fired with hard coal (fly ash W) and brown coal (fly ash E).

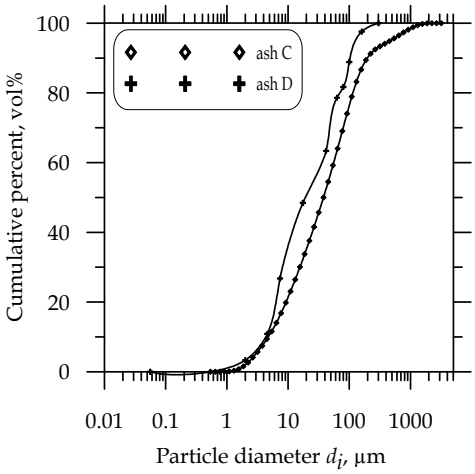

Fig. 7. Particle size distribution $Q_3(d_i)$ of fly ashes from PFB boilers fired with hard coal (fly ash C) and brown coal (fly ash D).

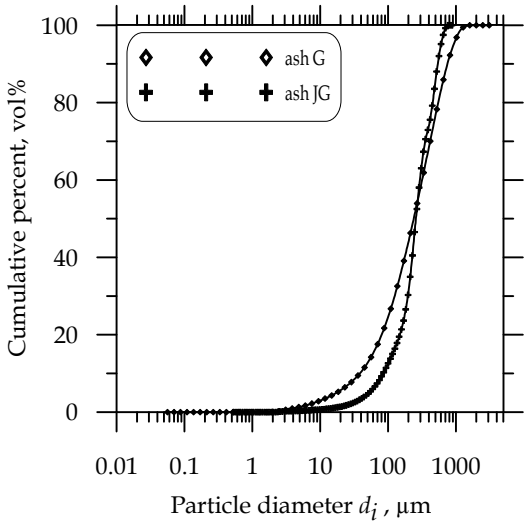

Fig. 8. Particle size distribution $Q_3(d_i)$ of fly ashes from grate stoker boilers fired with hard coal.

The influence of ESP device on fly ash size distribution is presented in Fig. 9. At the outlet of a high efficiency ESP (η_C>99.9 %), the fly ash comprises mainly of fine particles having diameter below 20 μm.

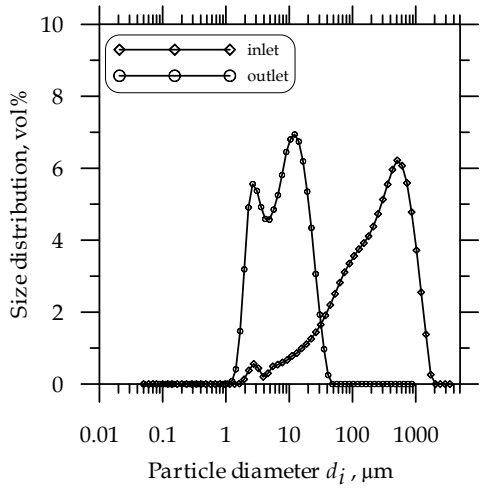

(a)

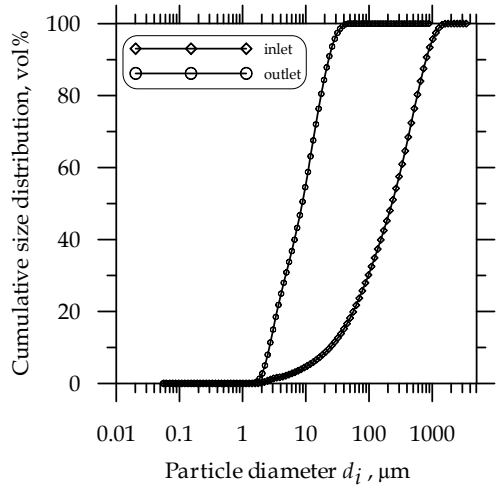

(b)

Fig. 9. Particle size distribution at an ESP inlet and outlet: (a) particles fraction $q_r(d_i)$, (b) cumulative size distribution $Q_3(d_i)$, fly ash from grate stoker boiler fired with hard coal.

4.3 Particle forms of a fly ash

Different methods of measuring fly ash size distribution utilize the same geometric parameter i.e. particle substitute diameter. But as it was mentioned before, the actual shape (form) of particles are rare spherical that also influences their separation process in an ESP.

In Fig. 10 are shown different particle-shape patterns, which can be found in various fly ashes: spherical forms (spherules) and sharp-edged (Fig. 10a), particles in the form of fibers

and particles with a very irregular shapes (Fig. 10b). Moreover there is also visible a significant particle size diversification. Scanning Electron Microscope (SEM) micrographs taken at high magnification show the complexity of the forms of particles, which are often agglomerates of many smaller particles having different diameters.

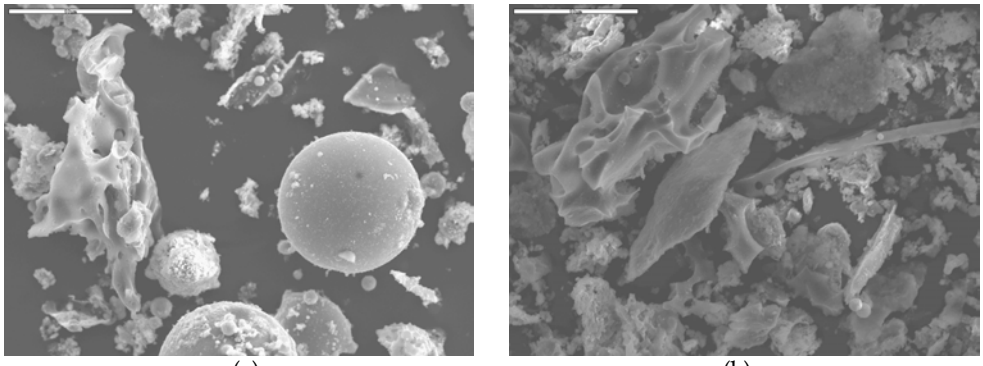

(a) (b)

Fig. 10. SEM pictures of fly ash particles from hard coal fired boilers: (a) in a grate stoker boiler (fly ash G), and in a PC boiler (fly ash C) (magnification 700x).

On the photo (Fig. 11) are shown characteristic shapes (forms) of fly ash particles coming from brown coal fired boilers with different combustor systems.

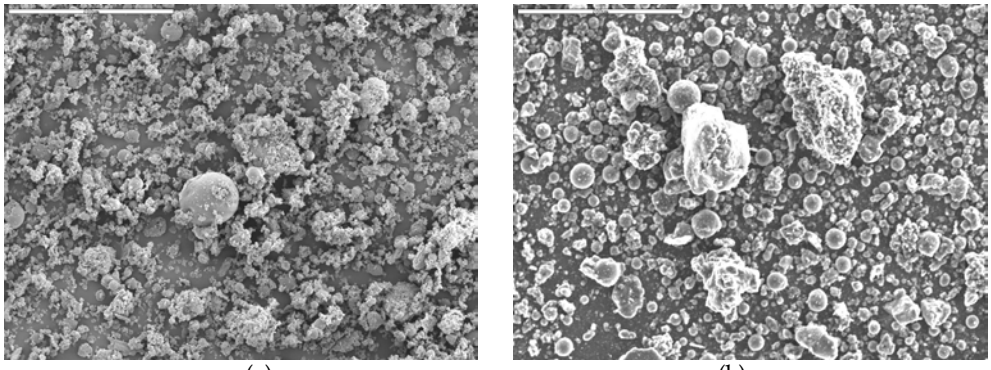

(a) (b)

Fig. 11. SEM pictures of fly ash particles coming from coal fired boilers: (a) brown coal fired in fluidal bed boiler (fly ash D), (b) brown coal fired in PC boiler (fly ash E) (magn. 230x).

The elemental analysis carried out by Energy Dispersive X-Ray spectroscopy (EDX) method demonstrates that most of the particles are alumina-silica (Al_2O_3-SiO_2) aggregates (Fig. 12) as well as spherical granules of two kinds: built of alumina-silica and spherical forms of iron oxides (Fig 13). In addition to that in the fly ash were found particles with compounds characteristic of carbonates, sulfates and oxides (quartz, feldspar, calcite and gypsum), with considerable addition of titanium, iron, potassium, calcium, plus small content of sulfur and potassium (Grafender, 2010).

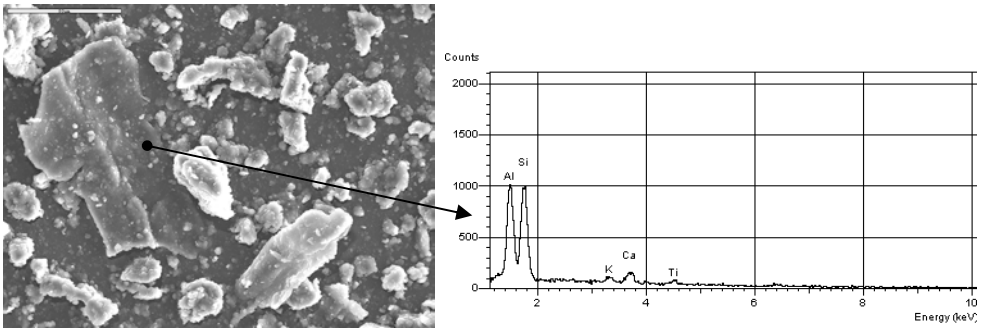

(a) (b)

Fig. 12. Fly ash particles composed of alumina-silicates (magn. 700x) - (a) and their elemental analysis - (b), fly ash from CFB boiler fired with brown coal (fly ash D).

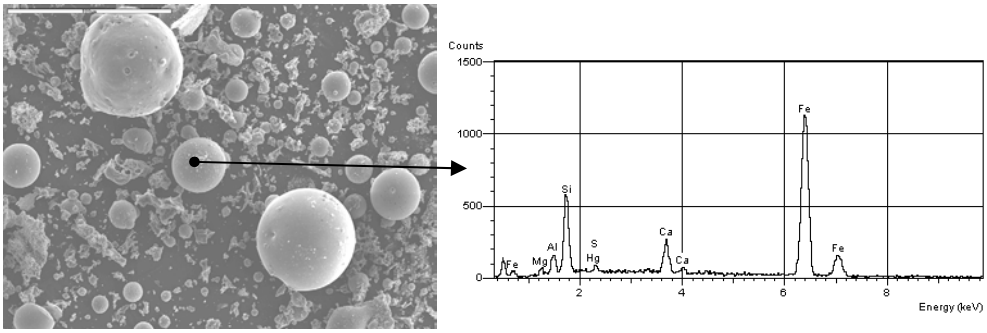

(a) (b)

Fig. 13. Fly ash particles of spherical form composed of iron-oxides (magn. 100x) - (a) and their elemental analysis - (b), fly ash from grate stoker boiler fired with hard coal (fly ash JG).

5. Discharge Electrode (DE) model investigation

5.1 Testing bench

The model investigations of discharge electrodes (DE) have been carried out in a laboratory arrangement comprised of pilot ESP with horizontal air flow, as shown on Fig. 14. The chamber is made of organic glass (2000 mm long, 400 mm wide and 450 mm high) that enables visual observations as well as photography of the phenomenon occurring in the inter electrode region.. Tests were carried out with air flow at a temperature of 20°C , pressure 1000 hPa and at humidity of 60% (Jędrusik & Świerczok, 2009).

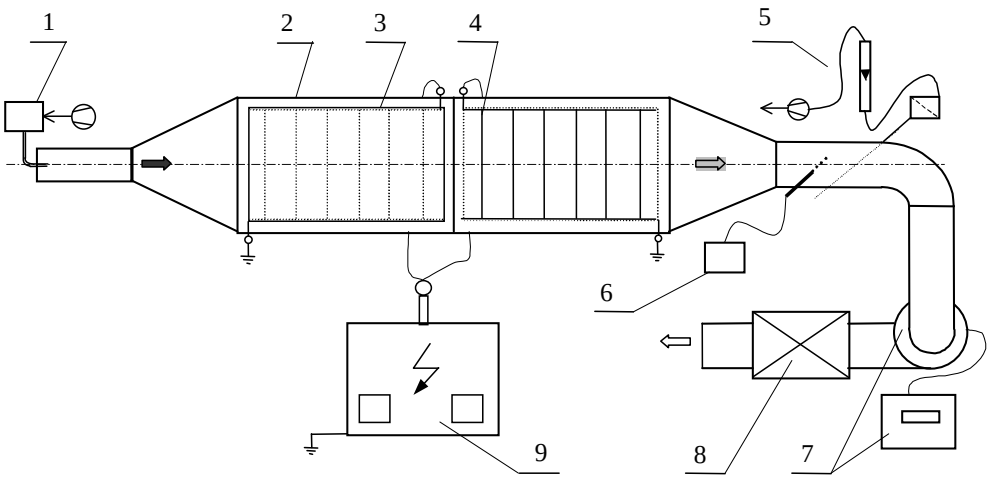

Fig. 14. Laboratory arrangement for DE testing in a pilot ESP : 1 – fly ash feeder, 2 – pilot ESP chamber, 3 – CE (collecting electrodes), 4 – DE (discharge electrodes), 5 – dust meter, 6 - thermo anemometer , 7 – exhaust fan with rotational speed control, 8 – final filter, 9 – HV (high voltage) supply unit.

5.2 V-I (voltage-current) characteristics

In Fig. 15 are shown various constructions of tested rigid discharge electrodes (RDE). In electrodes of this type, both functions of the construction: mechanical supporting and electric-discharge generation have been separated via mounting the active spikes as replaceable elements that allows replacement of the emission points without changing the supporting part. The V-I characteristics shown in Fig. 16 allows to divide the considered RDE constructions into two groups:

1. 'aggressive' (with steep V-I curve) – the so called 'RDE-3', having discharge onset at a level of U_0=10 kV and the 'barbed type' with higher onset voltage of about U_0=22 kV; and
2. 'smooth': RDE-1 with discharge onset level of U_0=16 kV and RDE-2 with U_0=14 kV (Jędrusik & Świerczok, 2011).

The tests have shown that modification of spikes orientation and spacing influences the V-I curvature, what can be seen in Fig. 17. That gives the possibility to select and optimize DE electrodes according to required precipitation efficiency and the expected shape of its V-I characteristic. This becomes important when fly ash parameters are changed (mainly its resistivity), for example, as a result of changing the kind fired fuel. Hitherto existing experience shows that for efficient precipitation of high-resistivity fly ash the DE construction should allow a high discharge voltage and uniform discharge current distribution. Such electrode is called " high voltage & moderate discharge current electrode".

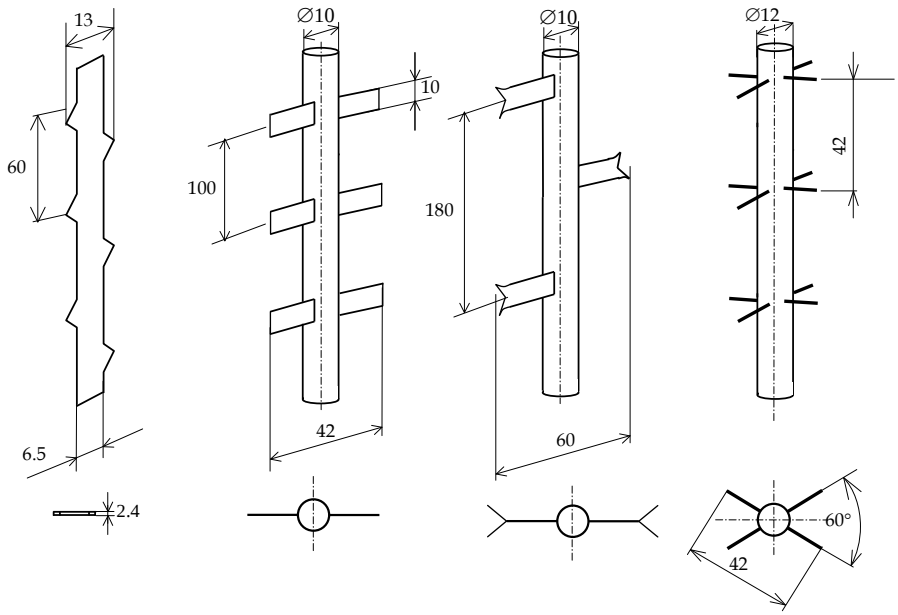

Fig. 15. Forms of discharge electrodes (DE): (a) 'barbed tape', (b) RDE–1, (c) RDE–2, (d) RDE–3.

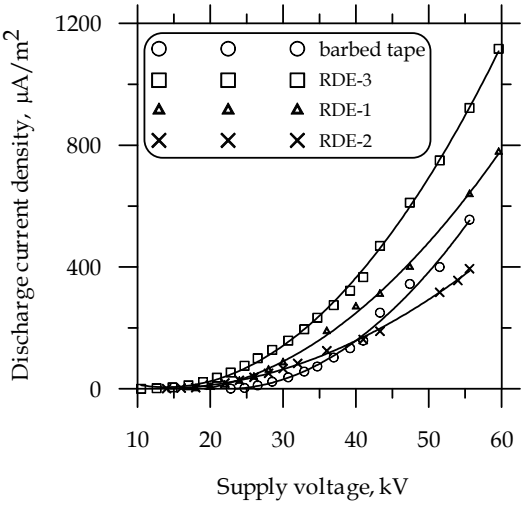

Fig. 16. V-I characteristics of DE electrodes shown on Fig. 15.

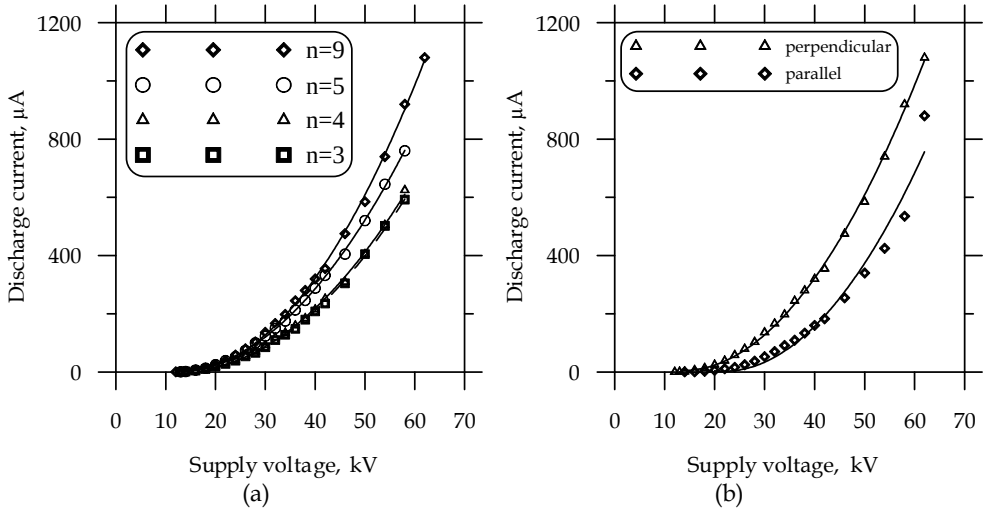

Fig. 17. V-I characteristics of RDE-2 electrode: (a) effect of discharge spikes number, (b) normal and parallel orientation of the spikes to the collection electrode CE.

At the end of 90s (of the 20th century) there were carried out many laboratory tests with various constructions of DE as well as with numerical modeling of phenomenon occurring in an electric discharge field regions for different 'spikes' of the electrodes (Brocilo et al., 2001; Caron & Dascalescu, 2004; Chung-Liang & Hsunling, 1999; Hsunling et al., 1994; McCain, 2001).

Regardless of those investigations, there still lack unambiguous criteria for the selection from various available constructions of DE. Very often ESPs are equipped with similar type of DEs irrespective on the gas-dust characteristic parameters or inter electrode spacing.

5.3 The influence of selected fly ash parameters on precipitation efficiency

In order to show the influence of fly ash chemical composition on precipitation efficiency a several measurements were done on a pilot ESP with selected fly ashes (parameters presented in Table 1) and selected DE constructions.

To illustrate the results, in Fig. 18 are shown characteristics of precipitation efficiency for three different fly ashes. The curves demonstrate that high content of compounds like Al_2O_3 (32.1%), SiO_2 (54.2%) with traces of SO_3 Na_2O in the fly ash decreases the ESP precipitation and efficiency -at the specific experiment conditions. For example, a 10% decrease of Al_2O_3 in the fly ash and increase of SO_3 up to 6% and Na_2O up to 1% cause an increase in the precipitation efficiency of fly ash that may indicate a favorable influence of sodium content in the fly ash (Jędrusik & Świerczok, 2006; Jędrusik, 2008).

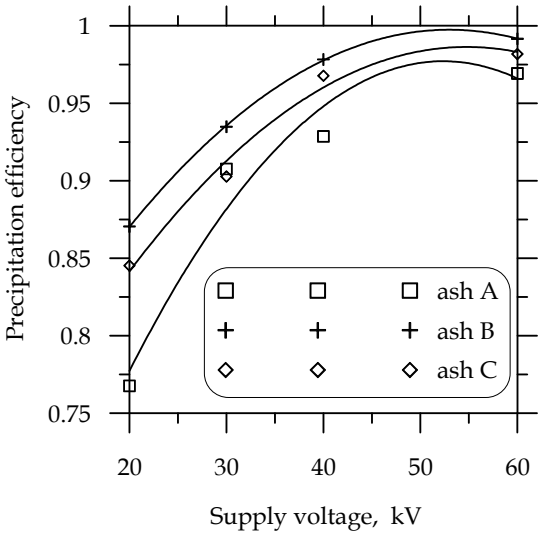

Fig. 18. Precipitation efficiency vs. supply voltage for RDE-2 electrode.

There was also tested the influence of unburned coal (LOI) content in fly ash on the precipitation efficiency, and an example of experimental results are presented in Fig. 19.

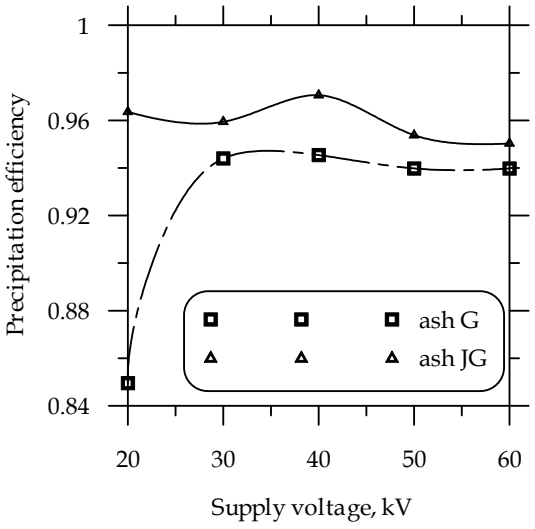

Fig. 19. Precipitation efficiency as a function of supply voltage for RDE-3 electrode and fly ash from hard coal fired grate stoker boiler.

The characteristics shown in Fig. 19 present the influence of unburned coal content in fly ash on the precipitation efficiency that was already observed in research works in 70'th of the 20th century. An increase of unburned coal percentage by over 15% decreased the precipitation efficiency (Hagemman & Ahland, 1973).

There was also tested the influence of biomass (of plant origin) co-firing in power boilers on precipitation process in the ESP, what is shown in Fig. 20.

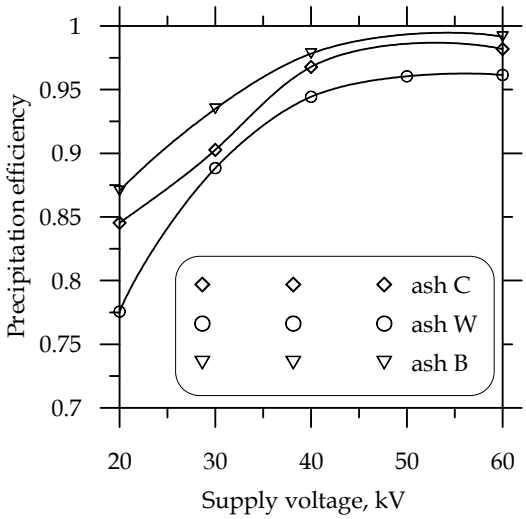

Fig. 20. The relationship between precipitation efficiency and a biomass percentage in the co-firing process (hard coal), RDE-2 electrode.

It is shown that the collection efficiency depends on electrical parameters of the supply voltage and the biomass percentage. The collection efficiency increases with an increase of the supply voltage of the discharge electrode, but it is saturated for a certain voltage magnitude, of about 50 kV, for that specific case. Further increase of the voltage can even cause a slight decrease of collection efficiency. It was also determined, that small addition of biomass (10%) to bituminous coal (ash B) causes an increase of the collection efficiency, whereas for higher content of biomass, 50% (ash W) or larger, the collection efficiency decreases. These preliminary results indicate that further research on the effect of co-fired biomass content on the collection efficiency is required in order to optimize the operational parameters of electrostatic precipitator (Jaworek et al, 2011).

The optimization of DE (corona electrode) design should include not only the parameters of the electric field, but also the physical and chemical properties of the fly ash. In summary, the choice of an appropriate design of the discharge electrode should be based on a thorough examination of the dust particles and flue gas properties.

5.4 Current density distribution and patterns of precipitated dust on (CE) electrodes

The measurements of current density enables better estimation of selected DE constructions especially in connection with local accumulation of fly ash on CE surfaces. The deposition of dust in an ESP creates collection patterns, which shape depends on the electric field forces in the inter-electrode space (Miller et al. 1996a, 1996b).

A measuring arrangement diagram is shown on Fig. 21.

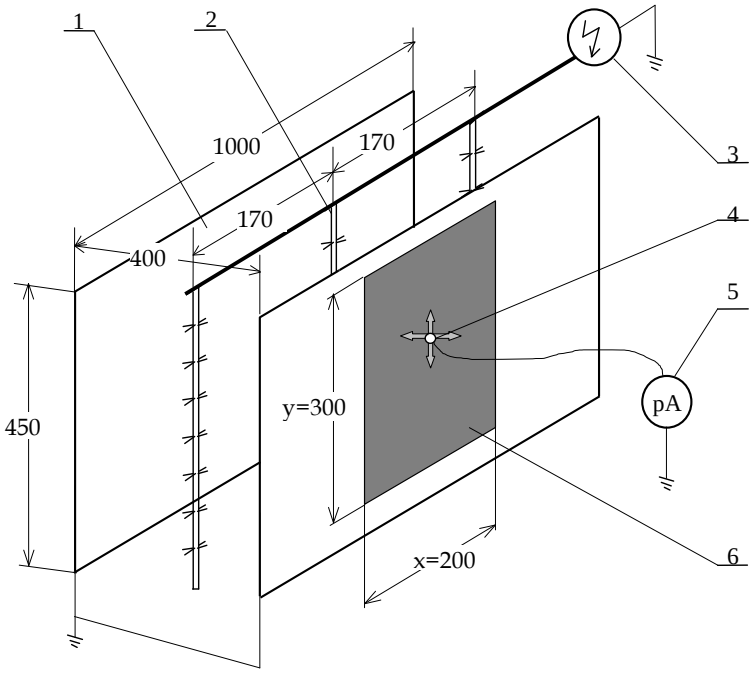

Fig. 21. Measuring arrangement of discharge current distribution on the CE surface:
1 – collecting electrodes, 2 – discharge electrodes, 3 – HV supply unit, 4 –measuring panel, 5 – pico-ammeter, 6 – measuring zone.

In Fig. 22 is presented discharge current distribution for RDE-3 electrode (Fig. 15d) with 'spikes' pointed perpendicularly at the surface of CE. In Fig. 23 is shown pattern of collected fly ash on CE electrodes for this DE construction.

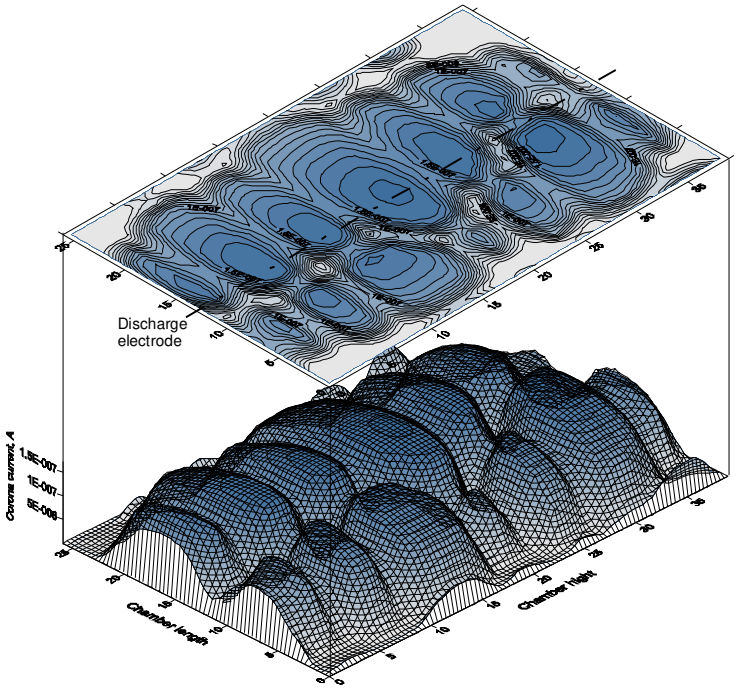

Fig. 22. Discharge current distribution for RDE-3 electrode - supply voltage 50kV.

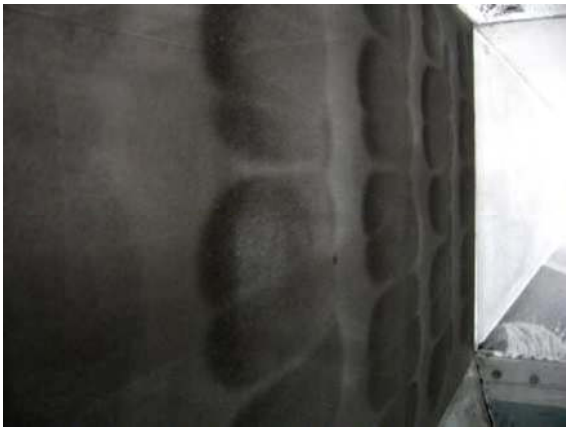

Fig. 23. Pattern of collected fly ash on CE electrodes for RDE-3 electrode.

From the results appears that the highest value of discharge current density is opposite the DE 'spike'. Hence the uniformity of discharge current distribution, which is important for high precipitation efficiency, will depend on the DE 'spikes' number and their configuration (Blanchard et al., 2002, McKinney et al., 1992). For this reason it is crucial to use DE

constructions, which limit the number and area of regions with very high or very low current density. Observation of the collection patterns on CE surfaces enables qualitative assessment of the discharge current distribution on the electrode. There is visible a significant correlation between the collected fly ash patterns and the measured distribution of discharge current. From the studies presented in (Miller et al., 1996a) also results that the collected fly ash layer density depends on the collection pattern, in which the highest density of the fly ash layer appears opposite the DE 'spikes', that should be related to the electric field distribution between the electrodes. This phenomenon may also be utilized in designing and selecting DE for collection of submicron particles.

6. Summary

The results presented in this Chapter have shown that different constructions of RDE electrodes in ESPs, their 'spike' number and geometrical configuration have to be used depending on physical and chemical properties of fly ash. Although the model studies have been carried out for only a few types of DE constructions and selected kinds of fly ashes, the experimental results, confirmed by the literature's data, had shown the influence of fly ash chemical composition as well as DE construction on the total collection efficiency of ESP. It was confirmed that some components of fly ash (e.g. Na_2O or Al_2O_3) have different effect on the collection efficiency, depending on DE construction and the type of fired coal (hard or brown coal). The results of measurements obtained for selected DE constructions in a pilot ESP have shown that the construction of DE, i.e., shape of their 'spikes', number of spikes, and their orientation relative to the collection electrode, have an influence on voltage-current characteristics and the corona onset voltage. These results suggest that voltage-current characteristics can be changed to some extent via changing the discharge electrode geometry (shape of spikes) or the modification of electrodes configuration. The possibility of the formation of V-I characteristics adequately to the existing collection conditions, enables more effective exploitation of H.V. supply units, in order to get higher collection efficiency of ESP and increasing energy efficiency of the supply unit. The presented results indicate also on new possibilities of more efficient removal of submicron particles in industrial ESPs.

7. References

Bibbo P.P. (1994). Agential flu gas conditioning for electrostatic precipitator, *Proc. of the American Power Conference,* Illinois Institute of Technology, USA, Vol. 56/V1,1994

Bickelhaupt R.E. (1985). A study to improve a technique for predicting fly ash resistivity with emphasis on the effect of sulfur trioxide, Prepared by U.S. EPA, Washington DC, 20460 SORI-EAS-85-841, November 1985

Blanchard D., Atten P., Dumitran L.M. (2002). Correlation between current density and layer structure for fine particle deposition in a laboratory electrostatic precipitator, *IEEE Transaction on Industry Applications*, Vol. 38, no. 3 May/June, pp. 832-839.

Brocilo C., Chang J.S., Findlay R.D. (2001). Modeling of electrode geometry effects on dust collection efficiency of wire-plate electrostatics precipitators, *Procee. 8th ICESP*, Vol. 1, Southern Comp. Services Inc., Birmingham, Alabama, USA, A4–3 Series, May 14–17, 2001

Caron A. & Dascalescu L. (2004). Numerical modeling of combined corona – electrostatics fields, *J. of Electrostatics*, Vol. 61, pp. .43-55

Chambers M., Grieco G.J., Caine I.C. (2001). Customized rigid discharge electrodes show superior performance in pulp & paper applications, *Procee. 8th ICESP*, Vol. 1, Birmingham, Alabama, USA, May 14–17, 2001

Chung-Liang Ch. & Hsunling B. (1999). An experimental study on the performance of single discharge wire-plate electrostatic precipitator with back corona, *J. Aerosol Sci*., Vol. 30, No. 3

Grafender A.M. (2010) Pyły atmosferyczne pod mikroskopem, *Energetyka Cieplna i Zawodowa*, 2/2010, pp. 22-25

Hagemann H. & Ahland E. (1973). Abgasentstaubug von mit Steinkohlenstaub gefeuerten Wasserrohr, *Staub-Reinhalt. Luft,* 33 (1973) Nr. 9, pp. 367-372

Hsunling B., Chungsying L., Chung-Liang Ch. (1994). A model to predict the system performance of an electrostatic precipitator for collecting polydispersed particles, *J. of Air and Waste Manage*, ASSOC, Vol. 45, pp. .908-916

IEEE-DEIS-EHD Technical Committee (2003). Recommended international standard for dimensionless parameters used in electrohydrodynamics, *IEEE Trans. Diel. Electr. Insul*. 10-1, pp. 3-6

Jaworek A., Jędrusik M., Świerczok A., Lackowski M., Czech T., Sobczyk A.T. (2011). Biomass co-firing. New challenge for electrostatic precipitators, *Procce. XII International Conference of Electrostatic Precipitation, ICESP XII*, Nuernberg, 10-13 Mai 2011

Jędrusik M. & Świerczok A. (2006). Experimental test of discharge electrode for collecting of fly ash of different physicochemical properties. *Procee. International Conference on Air Pollution Abatement Technologies – future challenges. ICESP X*, Cairns, Queensland, Australia, 25-29 June 2006,

Jędrusik M. (2008). *Elektrofiltry. Rozwinięcie wybranych technik podwyższania skuteczności odpylania*, Oficyna Wydawnicza Politechniki Wrocławskiej, ISBN 978-83-7493-387-2, Wrocław

Jędrusik M. & Świerczok A. (2009). The influence of fly ash physical & chemical properties on electrostatic precipitation process, *Journal of Electrostatics*, 67, pp. 105-109

Jędrusik M. & Świerczok A. (2011). The influence of unburned carbon particles on electrostatic precipitator collection efficiency, Journal of Physics: Conference Series 301 (2011) 012009, doi:10.1088/1742-6596/301/1/012009

Masuda H., Higashitani K., Yoshida H. (2006). *Powder Technology Handbook*, CRC Press Taylor & Francis Group, ISBN: 1-57444-782-3

Mc Kinney P.J., Davidson J.H., Leone D. M. (1992). Current distributions for barbed plate-to-plane coronas, *IEEE Transaction on industry Applications*, vol. 28, No.6 Nov/Dec, pp. 1424-1431

McCain J.D. (2001). Estimeted Operating V-I curves for rigid frame discharge electrodes for use In ESP modeling, *Procee. 8th ICESP*, Vol. 1, Birmingham, Alabama, USA, May 14–17, 2001

Miller J., Schmid H.J., Schmidt E., Schwab A.J. (1996a). Local deposition of particles in a laboratory-scale electrostatic precipitator with barbed discharge electrodes, *Procee. 6th International Conference on Electrostatic Precipitation*, Budapest, Hungary, 18-21 June 1996

Miller J., Schmidt E., Schwab A.J. (1996b). Improved discharge electrode design yields favourable EHD-field with low dust layer erosion in electrostatic precipitators,

Procee. 6-th International Conference on Electrostatic Precipitation, Budapest, Hungary, 18-21 June 1996

Parker K.R. (1997). *Applied Electrostatic Precipitation*, Blackie Academic & Prof., ISBN 07514 0266 4 London

Pauthenier M.M. & Moreau-Hanot M. (1932) La charge des particules spheriques dans un champ ionize, *Journal de Physique et le Radium*, 3, pp. 590-613

Peek F.W. (1929). *Dielectric phenomena in high voltage engineering*, 3rd ed., MacGraw-Hill, New York

White H.J. (1990). *Industrial Electrostatic Precipitation*, (prep.), International Society for Electrostatic Precipitation, Library of Congress Catalog Card No. 62-18240

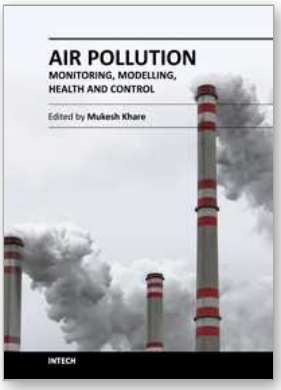

Air Pollution - Monitoring, Modelling, Health and Control

Edited by Dr. Mukesh Khare

ISBN 978-953-51-0381-3
Hard cover, 254 pages
Publisher InTech
Published online 21, March, 2012
Published in print edition March, 2012

Air pollution has always been a trans-boundary environmental problem and a matter of global concern for past many years. High concentrations of air pollutants due to numerous anthropogenic activities influence the air quality. There are many books on this subject, but the one in front of you will probably help in filling the gaps existing in the area of air quality monitoring, modelling, exposure, health and control, and can be of great help to graduate students professionals and researchers. The book is divided in two volumes dealing with various monitoring techniques of air pollutants, their predictions and control. It also contains case studies describing the exposure and health implications of air pollutants on living biota in different countries across the globe.

How to reference

In order to correctly reference this scholarly work, feel free to copy and paste the following:

Maria Jędrusik and Arkadiusz Świerczok (2012). Design Efficiency of ESP, Air Pollution - Monitoring, Modelling, Health and Control, Dr. Mukesh Khare (Ed.), ISBN: 978-953-51-0381-3, InTech, Available from: http://www.intechopen.com/books/air-pollution-monitoring-modelling-health-and-control/design-efficiency-of-esp-

INTECH
open science | open minds

InTech Europe
University Campus STeP Ri
Slavka Krautzeka 83/A
51000 Rijeka, Croatia
Phone: +385 (51) 770 447
Fax: +385 (51) 686 166
www.intechopen.com

InTech China
Unit 405, Office Block, Hotel Equatorial Shanghai
No.65, Yan An Road (West), Shanghai, 200040, China
中国上海市延安西路65号上海国际贵都大饭店办公楼405单元
Phone: +86-21-62489820
Fax: +86-21-62489821